RESEARCH

The Effect of Different Stabilisers on Stability and Photothermal Profiling of Gold Nanorods

Karabo Kamogelo Khoza[1,2] · Thabang Calvin Lebepe[1,2] · Gracia it Mwad Mbaz[1,2] · Oluwatobi Samuel Oluwafemi[1,2]

Abstract

The photothermal application of gold nanorods (AuNRs) as a photothermal agent has gained popularity due to their optical, photothermal and biological properties. However, AuNRs are synthesised using a biotoxic surfactant (cetyl trimethyl ammonium bromide) which limits their biological applications. Though different techniques have been established to address this challenge using different stabilizers or passivating agents, the effect of these stabilizers on AuNRs' colloidal stability, thermal stability, and photothermal conversion efficiency still need to be investigated. In this study, we evaluated the effect of different polymers or stabilisers; two synthetic polymers [methoxy polyethylene glycol thiol (mPEG-SH) and polyvinylpyrrolidone (PVP)] and one biopolymer (gelatin) on the stability and photothermal properties of AuNRs. AuNRs absorbing around 800 nm were synthesised and coated with these three stabilisers. The colloidal stability of the as-synthesised material was evaluated in Dulbecco's phosphate-buffered saline (PBS) and Roswell Park Memorial Institute (RPMI-1640) using Ultraviolet–Visible–Near-Infrared (UV–Vis–NIR). The results show that PEG@AuNRs was more stable in both media due to fewer functional groups on its structure to bond with ions and protein. PVP@AuNRs showed good thermal stability under heat incubation (at 37, 50 and 70 °C) for 24 h because of its high thermal decomposition properties, while PEG@AuNRs proved superior in improving the AuNRs heat generation. In addition, coating with different polymers did not affect the photothermal ability of AuNRs. This study demonstrated that it is crucial to choose polymers with less functional groups when coating nanoparticles for biological application.

Keywords Gold nanorods · Surface modification · Polyvinylpyrrolidone · Polyethylene glycol thiol · Gelatin · Stability

1 Introduction

Gold nanorods (AuNRs) are promising photothermal agents among gold nanomaterials because they absorb light and convert the energy into heat for cellular tumour damage, wound healing or killing bacterial infection [1, 2]. Their unique properties of producing a longitudinal surface plasmon resonance (LSPR) and a transverse surface plasmonic resonance (TSPR) are responsible for AuNRs' ability to absorb light [3–9]. The resonance of free electrons causes SPR absorption at the gold surface in the presence of incident radiation [1]. Therefore, AuNRs can be used as Raman enhancers to improve Raman scattering near the surface in a process known as Surface-Enhanced Raman Scattering (SERS) and as SERS substrate materials in biomedical imaging, detection and optical data storage [2]. They can also be used as a drug carrier and a photothermal material for synergistic cancer treatment [10].

Several methods have been developed to synthesise AuNRs; among them, the seed-mediated method is the most commonly used because it is easy to deploy [11, 12]. However, cetyltrimethylammonium bromide (CTAB), used as a surfactant, has been reported to be a biotoxic compound, which limits the AuNRs biological applications [12]. Thus different surfactants have been recommended via different approaches to replace CTAB on the surface of the AuNRs and reduce their toxicity while improving their stability [10]. These approaches can be grouped into ligand exchange, layer-by-layer, and encapsulation. To date, numerous materials have been deployed to modify/ functionalise the surface

✉ Oluwatobi Samuel Oluwafemi
oluwafemi.oluwatobi@gmail.com

1 Department of Chemical Sciences, University of Johannesburg, Doornfontein, P.O. Box 17011, Johannesburg 2028, South Africa

2 Centre for Nanomaterials Science Research, University of Johannesburg, Johannesburg 2028, South Africa

of AuNRs. For example, ligand exchange and layer-by-layer usually use synthetic polymers [13–17], biopolymers [18–20], and organic molecules [21]. While for encapsulation, materials such as Mxenes [22], proteins [23–25], and Oxides (mSiO$_2$ and graphene oxide) [1, 11, 26, 27] are used to improve the biomedical applications of AuNRs. Though some surface alterations are very effective, the techniques used are complex, costly, unstable and often time-consuming. In addition, some lack versatility, thermal stability and pose toxicity risks [1].

The functionlisation of AuNRs via ligand exchange techniques have gained popularity because they are cheap and easy to carry out, and many of the polymers used have been shown to reduce the toxicity of AuNRs [13–17]. This modification advance application of AuNRs as drug carriers [28–30], biocompatible photothermal agents [11, 28, 31–34] and contrast agents [35, 36] in biotechnology and nanomedicine field. Nonetheless, the comparison of the polymer's differences, such as the functional groups, and how they can affect their thermal stability, colloidal stability and photothermal efficiency need to be investigated. In this study, AuNRs were coated using different polymers; two synthetic polymers (mPEG-SH and PVP) with different functional groups and one biopolymer (gelatin) with similar functional groups as one of the synthetic polymer (PVP). This was followed by evaluating the effect of these polymer/stabilisers on the thermal, colloidal stability, and photothermal profiling of AuNRs. The colloidal stability was evaluated in two culture media; phosphate-buffered saline (PBS) and Roswell Park Memorial Institute (RPMI-1640). The thermal stability was investigated at different temperatures (37 °C, 50 °C and 70 °C) at different times. The heat-generating capacity after coating was evaluated by irradiation with an 808 nm laser set at 2.98 W/cm^2 until the highest constant temperature for each sample was reached. The study showed that coating AuNRs with fewer functional groups polymers could improve their colloidal stability compared to highly rich functional group polymers. Furthermore, the higher the polymer's heat dissociation temperature, the better the protection of AuNRs for both photothermal application and thermal stability in the body.

2 Materials and method

2.1 Materials

Cetyltrimethylammonium bromide (CTAB, ≥ 98%), hydrogen tetrachloroaurate hydrate (HAuCl$_4$·xH$_2$O, ≥ 99%), sodium borohydride (NaBH$_4$, ≥ 99%), sodium hydroxide (NaOH, 50% in H$_2$O), hydrochloric acid (HCl), silver nitrate (AgNO$_3$, ≥ 99%), ascorbic acid (≥ 99%), methoxy polyethylene glycol-thiol (mPEG-SH), polyvinylpyrrolidone (PVP),

gelatin, Roswell Park Memorial Institute (RPMI), supplemented with 10% fetal bovine serum, 1% L-glutamine–penicillin–streptomycin, and 0.5% geneticin) and phosphate-buffered solution (PBS, Ca^{2+} and Mg^{2+} free, pH = 7.4) were purchased from Sigma-Aldrich, Kempton Park, South Africa. All solutions of gold salt, AgNO$_3$ and NaBH$_4$ were freshly prepared, and the glassware used in the experiments was cleaned and washed thoroughly with aqua regia and dried before use.

2.2 Methodology

2.2.1 Gold Nanorods Synthesis

AuNRs were synthesised using the seed-mediated method with some modifications [5]. The seed solution was first prepared by mixing 0.5 mL of HAuCl$_4$.xH$_2$O (0.01 M) with 9.5 mL of CTAB (0.1 M) for 15 min, followed by the addition of 0.46 mL of freshly prepared ice-cold NaBH$_4$ (0.01 M) in 0.01 M NaOH. The solution was stirred for 10 min and left undisturbed at room temperature for more than 30 min. On the other hand, A growth solution was prepared by mixing 0.50 mL of HAuCl$_4$·xH$_2$O (0.010 M), 9 mL of freshly prepared CTAB (0.10 M), and 0.10 mL of AgNO$_3$ (0.010 M) in 15 min under continuous gentle stirring, respectively. 0.20 mL of HCl (1 M) was added, followed by 80 μL of ascorbic acid (0.10 M) and 1 mL of the seed solution. Finally, the solution was kept at room temperature for 16–20 h. The solution was purified using centrifugation at 4500 rpm for 30 min to remove the excess CTAB. The colourful supernatant was then transferred to a new centrifuge tube and concentrated by centrifugation at 14,000 rpm for 2 h. The as-synthesised AuNRs were analysed using Ultraviolet–Visible–Near-Infrared (UV–Vis–NIR) spectrophotometer, Fourier Transform Infrared Spectroscopy (FTIR), Dynamic Light scattering (DLS) and Transmission electron microscopy (TEM).

2.2.2 Coating of Gold Nanorods with Different Stabilisers

2.2.2.1 PEGylation of Gold Nanorods The AuNRs pegylation was done according to Niidome et al. with modifications [37]. Briefly, 2 mL of MPEG-SH (5 mM) was added to 4 mL AuNRs (2.0 a.u. at the LSPR peak) solution. The solution was then stirred for 24 h at room temperature. The samples were analysed using UV–Vis–NIR spectrophotometer, FTIR, DLS and TEM and stored for future experiments.

2.2.2.2 Polyvinylpyrrolidone Coating of Gold Nanorods The coating of AuNRs with PVP (0.1 mg/mL) was done using Lebepe et al. method with modifications [12]. Briefly, 2 mL of PVP solution was added to 4 mL AuNRs (2.0 a.u. at the LSPR peak) solution, and the solution was stirred overnight

at room temperature. The samples were analysed using UV–Vis–NIR spectrophotometer, FTIR, DLS and TEM and stored for future experiments.

2.2.2.3 Gelatin Coating of Gold Nanorods

The coating of AuNRs with gelatin was done according to Oladipo et al. with modification [20]. 2 mL of gelatin was added to 4 mL AuNRs (2.0 a.u. at the LSPR peak) solution, and the mixture was then stirred for 6 h at room temperature. The as-synthesised coated AuNRs were analysed using UV–Vis–NIR spectrometer, FTIR, DLS and TEM and stored for future experiments.

2.2.3 Medium Stability of the As-synthesised Coated Gold Nanorods

The stability of CTAB/PEG/PVP/Gel@AuNRs was evaluated in two culture media (RPMI and PBS, pH = 7.4) following Lebepe et al. method with modifications [27]. Briefly, 1 mL of coated AuNRs (LSPR absorbance was adjusted to 1.0 ± 0.5 a.u.) was added into 2 mL of RPMI. The absorbance was measured after 0, 5, 10, 15, 30, 60 min and 24 h. The same procedure was repeated for stability in PBS.

2.2.4 Thermal Stability of the As-synthesised Coated Gold Nanorods

The thermal stability of the as-synthesised coated AuNRs was done following Zou et al. and Lebepe et al. methods with modifications [12, 38]. Briefly, 2 mL of the as-synthesised coated AuNRs (LSPR absorbance was adjusted to 1.0 ± 0.5 a.u.) were added into separate vials with a lid, and the solutions were then incubated at various temperatures (37, 50 and 70 °C). The changes in temperature for each sample were monitored at different times (0, 5, 10, 15, 30, 60 min and 24 h) using UV–Vis–NIR absorption spectra.

2.2.5 Evaluation of the Heat Generating Capacity of the As-synthesised Coated Gold Nanorods

The laser response was evaluated by adding 2 mL of each of the as-synthesised coated AuNRs (absorbance adjusted to 1.0 ± 0.5 a.u. at the LSPR peak) separately in a cuvette. Each sample was irradiated with 808 nm laser (dst11-LUMICS-808 nm 27W continuous, Nd: YV04 air-cooled laser system, with 8 mm beam diameter, OsTech e. K., Berlin, Germany) set at 2.98 W/cm² for 10 min with thermocouple (RS-1384 PRO with K-type thermocouple) for recording the temperature changes every 30 s and the thermal images (FLIR E4 thermal camera) captured every 2.5 min for 10 min. The heat generating capacity was calculated by placing 2 mL of as-synthesised coated AuNRs solution into a cuvette, followed by irradiation with an 808 nm laser set at

1.5 W until the highest constant temperature for each sample was reached. The laser was then turned off to allow the samples to cool to the initial temperature. The temperature changes were measured using a thermocouple. The photothermal conversion efficiency was calculated following Li et al. [39] steps with modification and equation below:

$$PCE = \frac{hs(\Delta T \max) - QDis}{I(1 - 10^{-A808})}$$

where ΔTmax is the difference between the equilibrium temperature and the ambient temperature of the surrounding (22 °C), I is the laser power (1.5 W), and A_{808} is the absorbance of the sample at 808 nm.

2.2.6 Characterisation Techniques

The absorption spectra of all the as-synthesised materials were obtained from a JASCO V-770 UV–Vis–NIR spectrophotometer (JASCO Corp., Tokyo, Japan). Microtrac MRB's NANOTRAC Wave II (Verder-Scientific Pty Ltd, Johannesburg, South Africa) was used to obtain the hydrodynamic size distribution of the as-synthesised materials. TEM images and morphologies of the as-synthesised AuNRs were captured using JEOL 2010 high-resolution transmission electron microscopy (200 kV, Tokyo, Japan). Five images were captured for each sample, and data were analysed using free ImageJ software (50 AuNRs/sample). The functional groups on the surface of AuNRs were analysed using the Perkin Elmer spectrum-II UATR spectrometer (Perkin Elmer, Midrand, South Africa).

3 Results and Discussion

3.1 Gold Nanorods Synthesis and Coating with Different Stabilisers

Gold nanorods (AuNRs) were synthesised using the seed-mediated method [5], purified by centrifugation for 30 min at 4500 rpm and concentrated at 14,000 rpm for 2 h. After 30 min of centrifugation at 4500 rpm, the sediment was a mixture of white and reddish in colour. This could be attributed to the presence of excess CTAB and big nanoparticles. The supernatant was further centrifuged at 14,000 rpm. After centrifugation, both the new sediment and supernatant were analysed using UV–Vis–NIR. Figure 1a shows that the LSPR wavelength positions of the supernatant and sediment were 763 nm and 800 ± 20 nm. The sediment was used for the coating with the different stabilizers.

The coating of the as-synthesised AuNRs with PVP, PEG, and Gel was confirmed using UV–Vis–NIR, DLS, TEM and FTIR. The UV–Vis–NIR spectra of PEG@AuNRs (Fig. 1b)
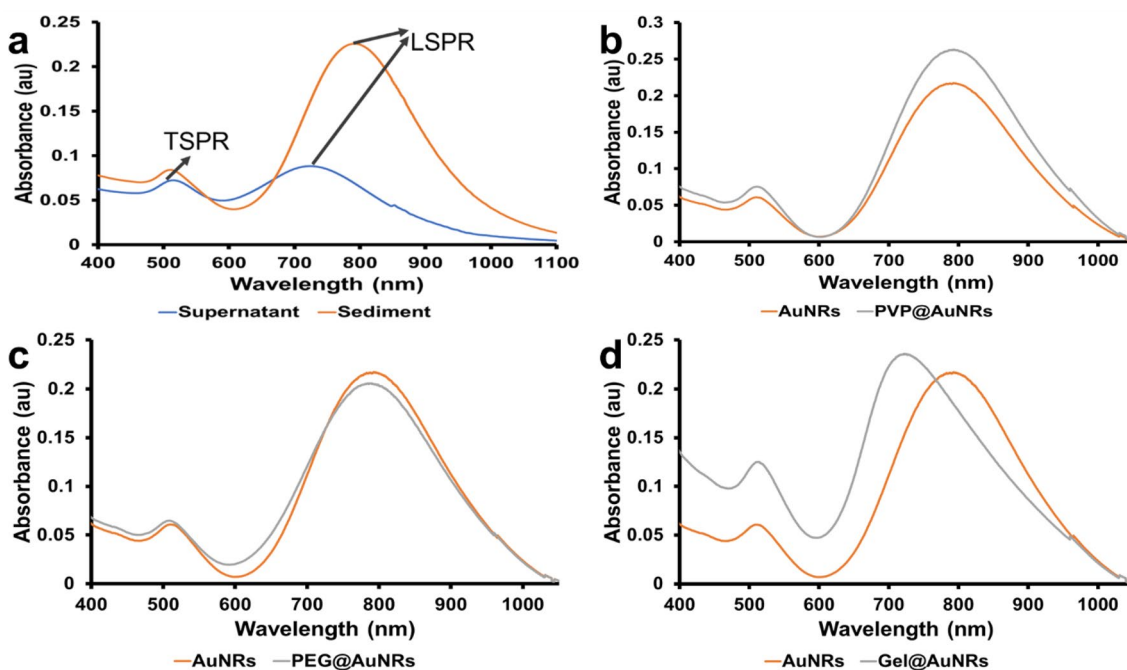
Fig. 1 **a** UV–Vis–NIR spectra of the supernatant and sediment after centrifugation at 14,000 rpm. UV–Vis–NIR spectra of AuNRs coating with **b** PVP, **c** PEG and **d** Gel

show that the intensity of the LSPR peaks decreased after coating compared to the bare-AuNRs (CTAB@AuNRs). In contrast, there was no significant shift in the LSPR peak wavelength after coating of AuNRs with PVP (PVP@ AuNRs, Fig. 1b). On the other hand, a blue shift of ~ 7 and ~ 76 nm was observed after coating with PEG and gelatin, respectively. According to the literature, the slight shift from PEG-coated AuNRs (PEG@AuNRs, Fig. 1c) could be attributed to the strong binding of the PEG thiol units to the AuNRs surface [37], while the shift from gelatin-coated AuNRs (Gel@AuNRs, Fig. 1d), could be attributed to the encapsulation of AuNRs by gelatin [1].

The as-synthesised nanomaterials were analysed using TEM to determine their morphology and aspect ratios before and after coating. The TEM micrographs of the as-synthesised AuNRs showed rod-shaped with some spheres (Fig. 2a); using image-J software, the average size distribution obtained was $20.8 \pm 3.9 \times 5.4 \pm 0.9$ nm with an aspect ratio of 3.89 nm (Fig. 2a, inset). Under high-resolution, lattice fringes were observed (Fig. 2a, inset), which confirms that the AuNRs are highly crystalline. The lattice fringe spacing of the CTAB@AuNRs obtained was 0.23 nm, which corresponds to the gold (Au) lattice plane {111} [20].

The coated AuNRs were also analysed using TEM. The results were similar to CTAB@AuNRs (Fig. 2b–d, Table S1). The lattice fringe spacing of PVP@AuNRs, PEG@AuNRs, and Gel@AuNRs was the same as the one for CTAB@AuNRs (Fig. 2b–d, inset). Since it is difficult to

accurately differentiate between the particle diameter using the TEM due to their close resemblance, the samples were then analysed with the DLS to determine their zeta potential and hydrodynamic sizes. The hydrodynamic size distribution of CTAB@AuNRs obtained from the DLS was 28.63 nm (Fig. 3a), which corresponded with the length size distribution obtained from the TEM micrograph. The smaller size peak observed on the DLS histogram is attributed to the rotational diffusion, which is influenced by the aspect ratio of the nanorods [40]. After coating with PVP, PEG and gelatin, the hydrodynamic size increased due to the change in the reflective index of the stabilisers (Fig. 3b–d). The high increase in size observed for Gel@AuNRs can be attributed to the encapsulation of the AuNRs after coating (Fig. 3d) [41]. The zeta potential of CTAB@AuNRs was positive at + 35.5 mV. However, after coating with PVP, PEG and Gel, the charge decreased to + 32.8, + 28.8 and + 15.9, respectively. The decrease in the surface charge could be attributed to the negative charge of the stabilisers. These results confirm that AuNRs was successfully coated with PVP, PEG and gelatin.

The changes in the functional groups on the surface of the coated AuNRs compared to the CTAB@AuNRs were evaluated using FTIR (Fig. 4) to further confirmed the coating. The FTIR spectra of CTAB@AuNRs showed the N–H stretch and O–H stretch at 3399 and 3018 cm^{-1}, respectively, C–H stretches at both 2917 and 2815 cm^{-1}, C=O stretch at 1725 cm^{-1}, C–H bends at 1463 cm^{-1} and a C–N stretch at
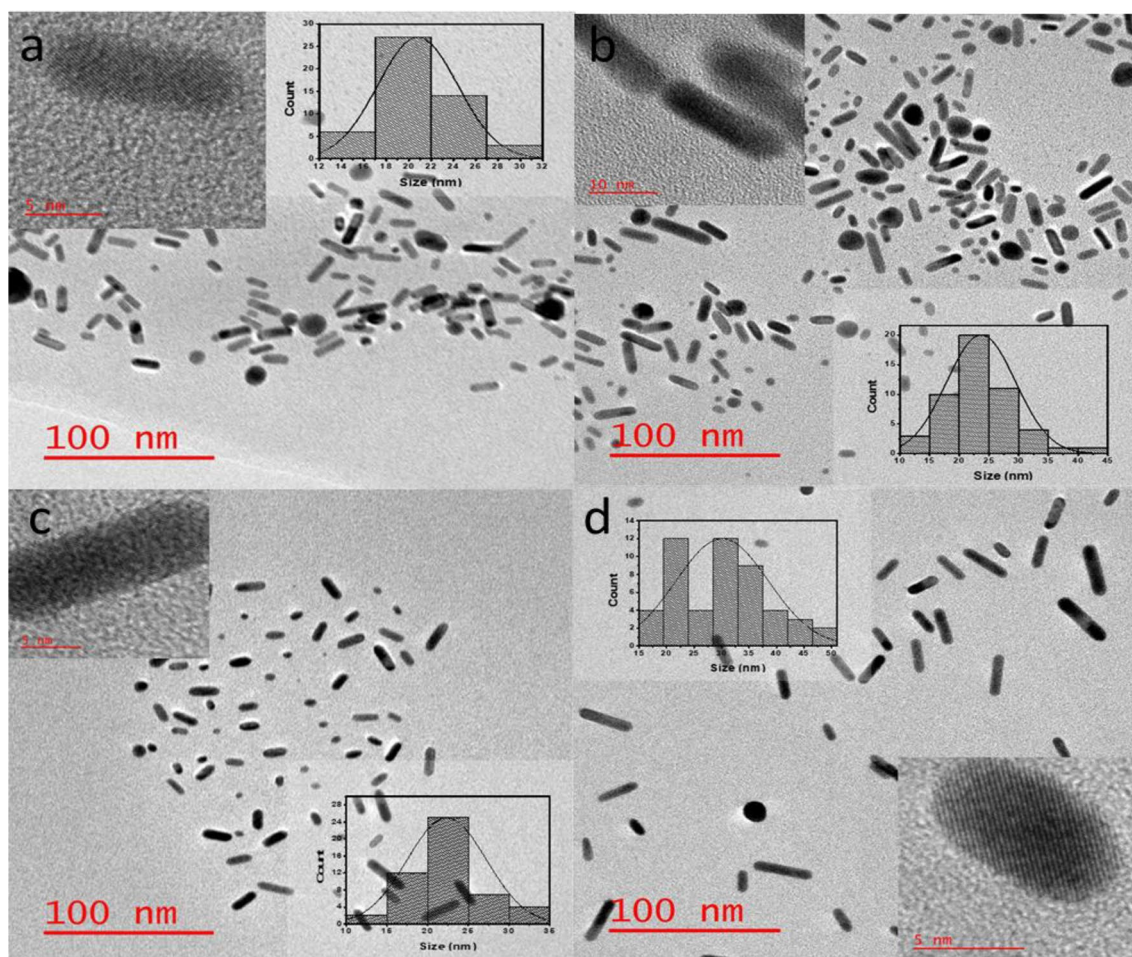
Fig. 2 TEM images of **a** CTAB@AuNRs, **b** PVP@AuNRs, **c** PEG@AuNRs and **d** Gel@AuNRs (Scale: 100 nm, inset: Particle size distribution and HRTEM images, scale 5 and 10 nm)

1245 cm^{-1} which are all attributed to the CTAB on the surface of CTAB@AuNRs [12]. The FTIR spectra of PVP@AuNRs and Gel@AuNRs showed almost similar peaks due to the similarity in their structural and functional groups. Both had strong C=O (1639 cm^{-1}) and C–N vibrations at 1345 and 1286 cm^{-1}, respectively, which are not seen in the CTAB@AuNRs spectrum. However, the Gel@AuNRs have two other amide vibrations at 1541 and 1238 cm^{-1}, which are not seen in PVP@AuNRs and CTAB@AuNRs. The PEG@AuNRs also showed slightly different peaks from CTAB@AuNRs with a formation of a new peak at 841 cm^{-1} from the –C–SH band found in m-PEG-thiol and shifting of C–O stretch at both 1280 and 1113 cm^{-1}. These results also show that the ligand exchange of CTAB to PVP, PEG and encapsulation with gelatin was successful.

3.2 Medium Stability of the As-synthesised Coated Gold Nanorods

The medium stability of the as-synthesised coated AuNRs in RPMI at room temperature was monitored at 0, 5, 10, 15, 30, 60 min, and 24 h. The LSPR peak of the samples blue-shifted at 5 min post dispersion in the medium (Fig. 5a, c, e, g). It is well known that RPMI contains different proteins; thus, the shift could be attributed to protein binding on the surface of as-synthesised coated AuNRs [12]. After 5 min, a slight decrease in the LSPR peak was observed with increasing TSPR band intensity which overlapped with the RPMI phenol red indicator peak at 561 nm. The reduction in the LSPR peak intensity indicates a decrease in the number of rods due to the surface interference of the stabilisers
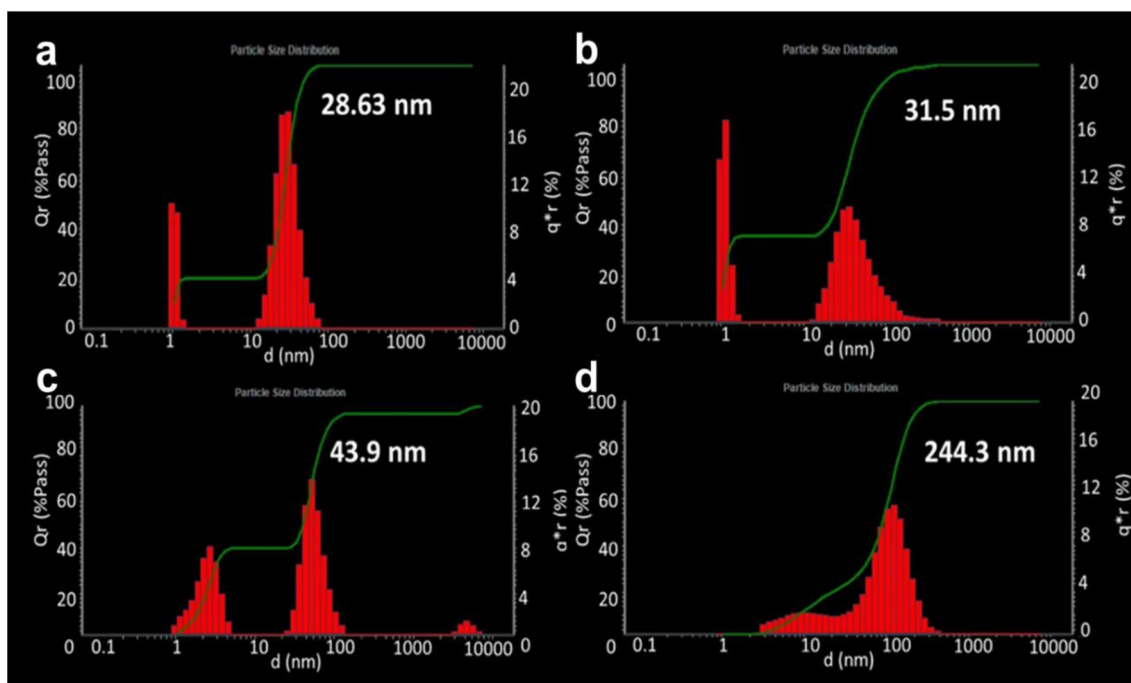
Fig. 3 Hydrodynamic size distribution of **a** CTAB@AuNRs, **b** PVP@AuNRs, **c** PEG@AuNRs and **d** Gel@AuNRs
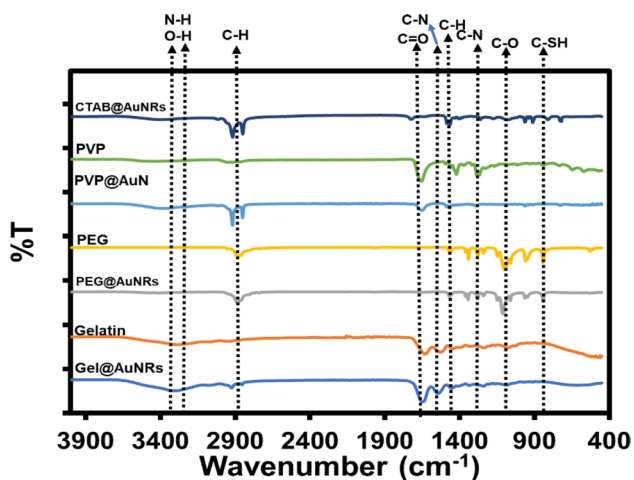

Fig. 4 FTIR spectra of CTAB@AuNRs, PVP, PVP@AuNRs, PEG, PEG@AuNRs, gelatin and Gel@AuNRs

via protein binding. This causes aggregation, which can be seen with increasing TSPR/phenol red peak. The CTAB@AuNRs (Fig. 5a) and PEG@AuNRs (Fig. 5e) stability compared to PVP@AuNRs (Fig. 5c) and Gel@AuNRs (Fig. 5g) can be attributed to the structural and functional groups. The PVP@AuNRs and Gel@AuNRs have C=O functional groups, which can strongly attract different proteins and lead to the aggregation of AuNRs.

A different medium without proteins was used to confirm the stability. All the as-synthesised coated AuNRs were

dispersed in PBS, following a similar procedure used for RPMI. The LSPR band of all the as-synthesised materials in PBS did not show a significant shift in wavelength (Fig. 5b, d, f, h) compared to the result obtained with RPMI (Fig. 5a, c, e, g). However, The LSPR band intensity of CTAB@AuNRs and PVP@AuNRs slightly decreased after 60 min and significantly at 24 h (Fig. 5b, d). The PEG@AuNRs did not show any significant changes in the spectra over time until 24 h, which cannot be attributed to structural changes in AuNRs (Fig. 5f). The stability of PEG@AuNRs over time can be attributed to the Au affinity to the thiol group. The Gel@AuNRs absorbance, on the other hand, increased with time because of the adsorption of varying ions present in the PBS solution (Fig. 5h). This behaviour of gelatin nanoparticles to adsorb ions has been reported, and it is used in water purification to remove metals [42]. From these results, we can infer that the more functional groups a stabiliser has, the lower the AuNRs' stability. The PEG@AuNRs with fewer functional groups is more stable compared to PVP@AuNRs and Gel@AuNRs with high electronegative functional groups. The PEG@AuNRs does not allow easy binding with proteins and other ions. Hydrodynamic sizes analysis showed that the RPMI and PBS contents were interacting with the coated AuNRs showing broader peaks (Figs. S1–S3) compared to the original peaks (Fig. 3b–d). However, the Gel@AuNRs showed a smaller size peak intensity change, which can be attributed to the aspect ratio of the nanorods changes, which correspond to the UV–Vis–NIR reported earlier. For future perspective, we recommend that
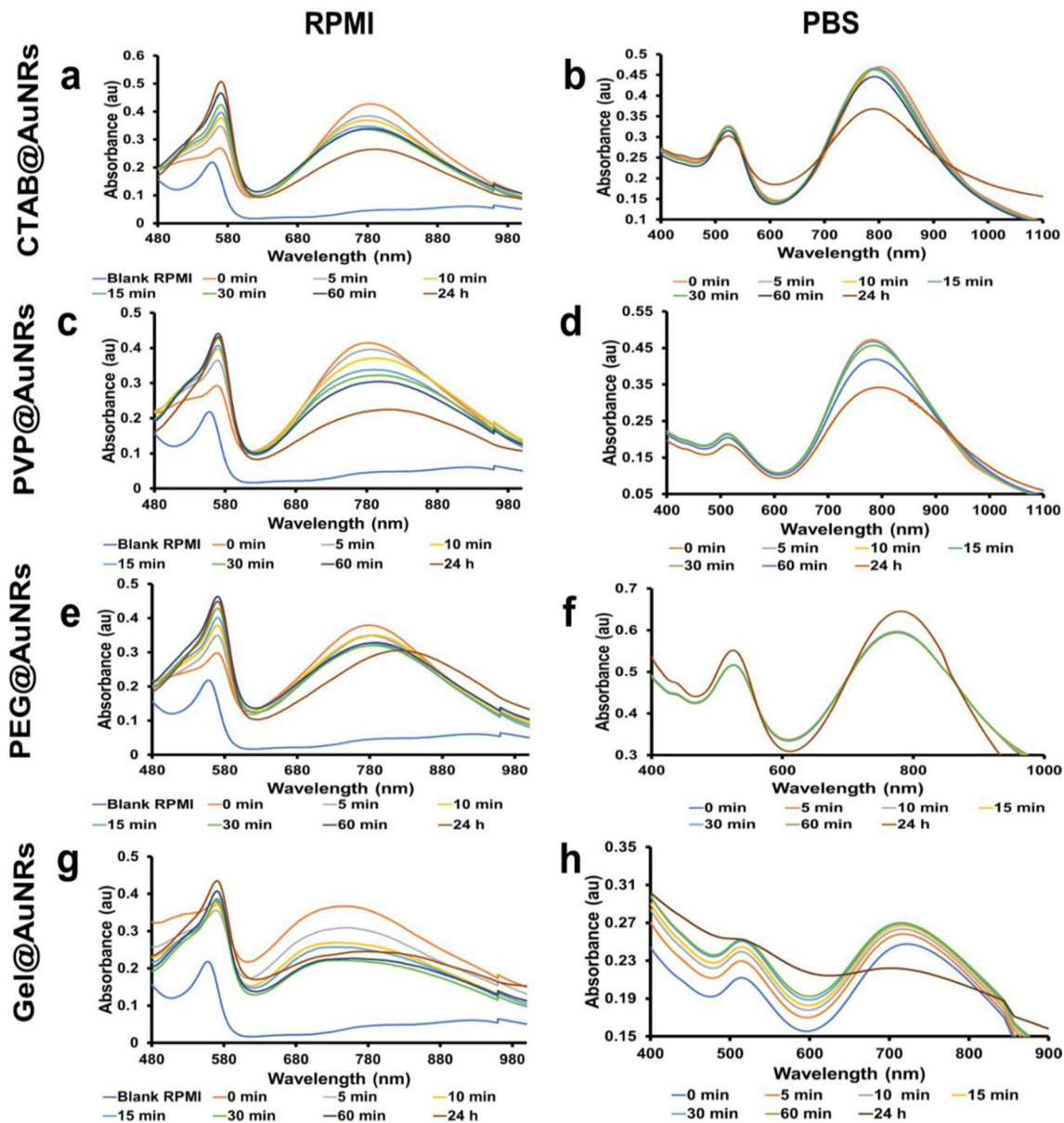
Fig. 5 UV–Vis–NIR spectra of **a**, **b** CTAB@AuNRs, **c**, **d** PVP@AuNRs, **e**, **f** PEG@AuNRs and **g**, **h** Gel@AuNRs dispersed into RPMI and PBS medium at different times

another polymer with similar functional groups as thiolated-PEG (e.g. thiolated poly(2-oxazolines) can be investigated to see if the thiol group's stronger affinity to Au with other polymers will give similar results.

3.3 Thermal Stability of the As-synthesised Coated Gold Nanorods

In photothermal application, it is important for photothermal agents to convert light energy into heat, raise the surrounding tissue's temperature and cause cell or bacterial death. In addition, for the materials to be used in the body, they must

not only withstand the body's physico-chemicals but also the body temperature. The as-synthesised materials were incubated at different temperatures for 0, 5, 10, 15, 30, 60 min, and 24 h to observe which stabiliser could withstand body temperature and high temperatures. The starting temperature was 37 °C, chosen because it is an average body temperature. The UV–Vis–NIR spectra of CTAB@AuNRs (Fig. 6a) and PVP@AuNRs (Fig. 6b) showed stability with barely reduced LSPR peak intensity. On the other hand, PEG@AuNRs became reduced after 30 min (Fig. 6c), while Gel@AuNRs was the least stable. Its LSPR peak absorbance was reduced, and its wavelength was blue-shifted in the first 10 min after
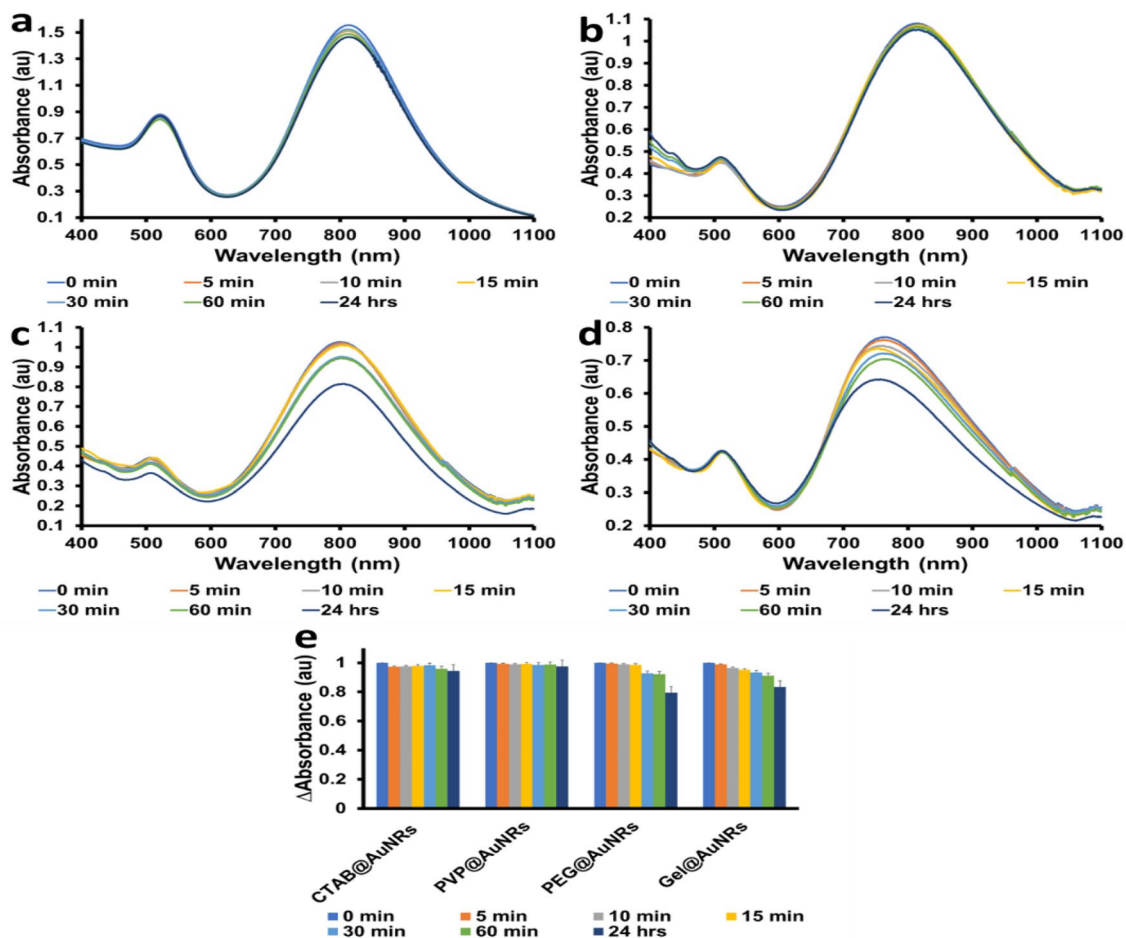
Fig. 6 UV–Vis–NIR spectra of **a** CTAB@AuNRs, **b** PVP@AuNRs, **c** PEG@AuNRs and **d** Gel@AuNRs and **e** change in absorbance of CTAB@AuNRs, PVP@AuNRs, PEG@AuNRs and Gel@AuNRs after heating at 37 °C at different times

incubation (Fig. 6d). This reduction in the absorbance indicates a change in the rods' morphology [38, 43]. CTAB@AuNRs and PVP@AuNRs LSPR peak absorbance had less than a 5% decrease after 24 h of incubation, whereas the Gel@AuNRs gradually decreased with time. It was reduced by 17% after 24 h (Fig. 6e). Conversely, PEG@AuNRs was the least, with a 20% decrease after 24 h.

The thermal stability of all the as-synthesised AuNRs was further investigated at 50 °C and 70 °C. The 50 °C was chosen because this temperature only affects the cancer cells [44]. The UV–Vis–NIR spectra of all the as-synthesised AuNRs after incubating at 50 °C over time are shown in Fig. S4. The results show that the LSPR wavelength positions for CTAB@AuNRs (Fig. S4a), PVP@AuNRs (Fig. S4b), PEG@AuNRs (Fig. S4c) and Gel@AuNRs (Fig. S4d) were stable at this temperature for an hour with a slight decrease in absorbance. The LSPR absorbance at 50 °C shows that PVP@AuNRs was stable with only a 7% decrease, followed by CTAB@AuNRs at 12%, Gel@AuNRs at 19%, and the least was PEG@AuNRs, 36% at 24 h of incubation (Fig. 7a).

The samples were further incubated at 70 °C. The results show that the LSPR peak positions of CTAB@AuNRs (Fig. S5a), PVP@AuNRs (Fig. S5b) and PEG@AuNRs (Fig. S5c) were still stable at this temperature over 60 min. The results also show that the LSPR intensity for CTAB@AuNRs, PVP@AuNRs and PEG@AuNRs were stable for an hour (Fig. 7b). However, after 24 h, the three samples showed a significant decrease in the LSPR absorbance. In addition, PEG@AuNRs also showed a significant blue shift in the LSPR peak position. The blue shift in the PEG@AuNRs LSPR is a sign that the rod aspect ratio has changed (Fig. S5c) [38]. The CTAB@AuNRs was slightly unstable with only a 7 nm blue-shifted position at 24 h. This slight decrease could be attributed to the high decomposition temperature (200 °C) of CTAB [45]. However, the fact remains that CTAB is toxic for biological applications.

In contrast, PVP@AuNRs LSPR peak position did not show any shift at 24 h. Still, only a 15% decrease in intensity (Fig. S5b, Fig. 7b). The thermal stability of PVP@AuNRs has been attributed to the thermal stability of PVP up to
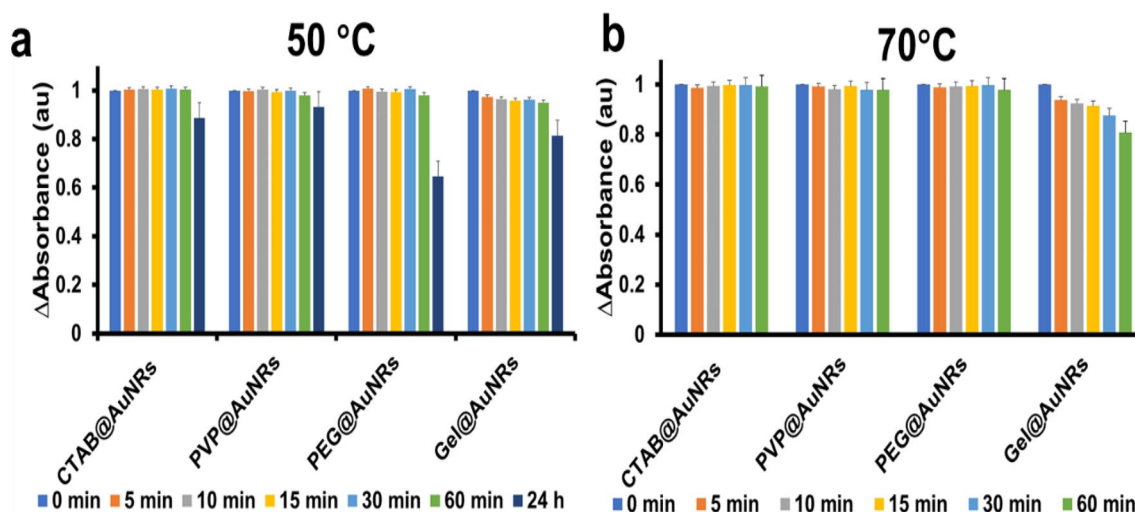
Fig. 7 LSPR intensity of CTAB@AuNRs, PVP@AuNRs, PEG@AuNRs and Gel@AuNRs after heating at **a** 50 °C and **b** 70 °C at different times

500 °C [46]. On the other hand, Gel@AuNRs LSPR absorbance and wavelength decreased during thermal treatment, indicating that the heating process changed the morphology of the rods (Fig. S5d, Fig. 7b) [43]. At 24 h, the LSPR band of Gel@AuNRs has completely disappeared, and the TSPR peak is broad (Fig. S5d). This could be attributed to the formation of bigger spheres or aggregation of the rods due to the heat, which gradually excited the water molecules. This weakened and broke the gelatin bonds leading to gelatin leaching on the surface of AuNRs. Thus, exposing the AuNRs to heat and causing them to aggregate [47].

3.4 The Heat-Generating Capacity of the As-synthesised Coated Gold Nanorods

The heat-generating capacity of the as-synthesised AuNRs was investigated with deionised water as a reference using an 808 nm laser set at 1.5 W (2.98 W/cm^2). The temperature changes were captured using a thermocouple and thermal camera. The thermocouple was set to record at an interval of 30 s for 10 min. The deionised water without nanomaterial was first irradiated. The results showed the temperature increased by 8.3 °C for 10 min when recorded from a thermocouple (Fig. 8a). When CTAB@AuNRs was irradiated for 10 min, the temperature change recorded was 26.4 °C. At the same time, PVP@AuNRs, PEG@AuNRs, and Gel@AuNRs produced temperature changes of 28.4 °C, 35 °C and 24.5 °C, respectively (Fig. 8a, Table S2). The ability of PEG to improve AuNRs thermal response could be attributed to PEG's excellent heat storage capacity that supports a higher temperature gradient compared to other surfactants [48].

The thermal camera images in Fig. 8b show the actual temperature of the as-synthesised material compared

to water. The images also show a similar trend as those observed on the thermocouple. The PEG@AuNRs is the highest, followed by PVP@AuNRs, CTAB@AuNRs and lastly, Gel@AuNRs. It is worth noting that the thermal camera recorded lower temperatures than the thermocouple because of the differences in emissivity and the camera's observation of the surrounding temperature [49]. The photothermal conversion efficiency (PCE) of the as-synthesised nanomaterials was also calculated using the linear plots (Fig. 8c–f) obtained from the cooling curve after each sample reached its temperature equilibrium (Fig. S6, Table S3) and the equation described in Sect. 2.2.5. The results are 28.7%, 34.10%, 48.6%, and 28.4% for CTAB@AuNRs, PVP@AuNRs, PEG@AuNRs, and Gel@AuNRs, respectively. These results agree with the earlier recorded temperature changes, with PEG@AuNRs having the highest heat production. These results suggest that all the materials do not affect the AuNRs' ability to produce heat. In addition, PEG heat storage capacity improves the photothermal conversion efficiency when binding to AuNRs.

4 Conclusions

In summary, AuNRs were successfully synthesised using the seed-mediated method followed by coating with three stabilisers (PVP, PEG and gelatin). The temporal evolution of the functional groups' effect on the AuNRs' colloidal stability, thermal stability and photothermal efficiency were investigated. The as-synthesised AuNRs had two absorption peaks at 513 nm and 800 ± 20 nm, with a hydrodynamic size of 28.6 nm. After coating the AuNRs with PEG and gelatin, the LSPR peak became blue-shifted by 7 nm and 76 nm,
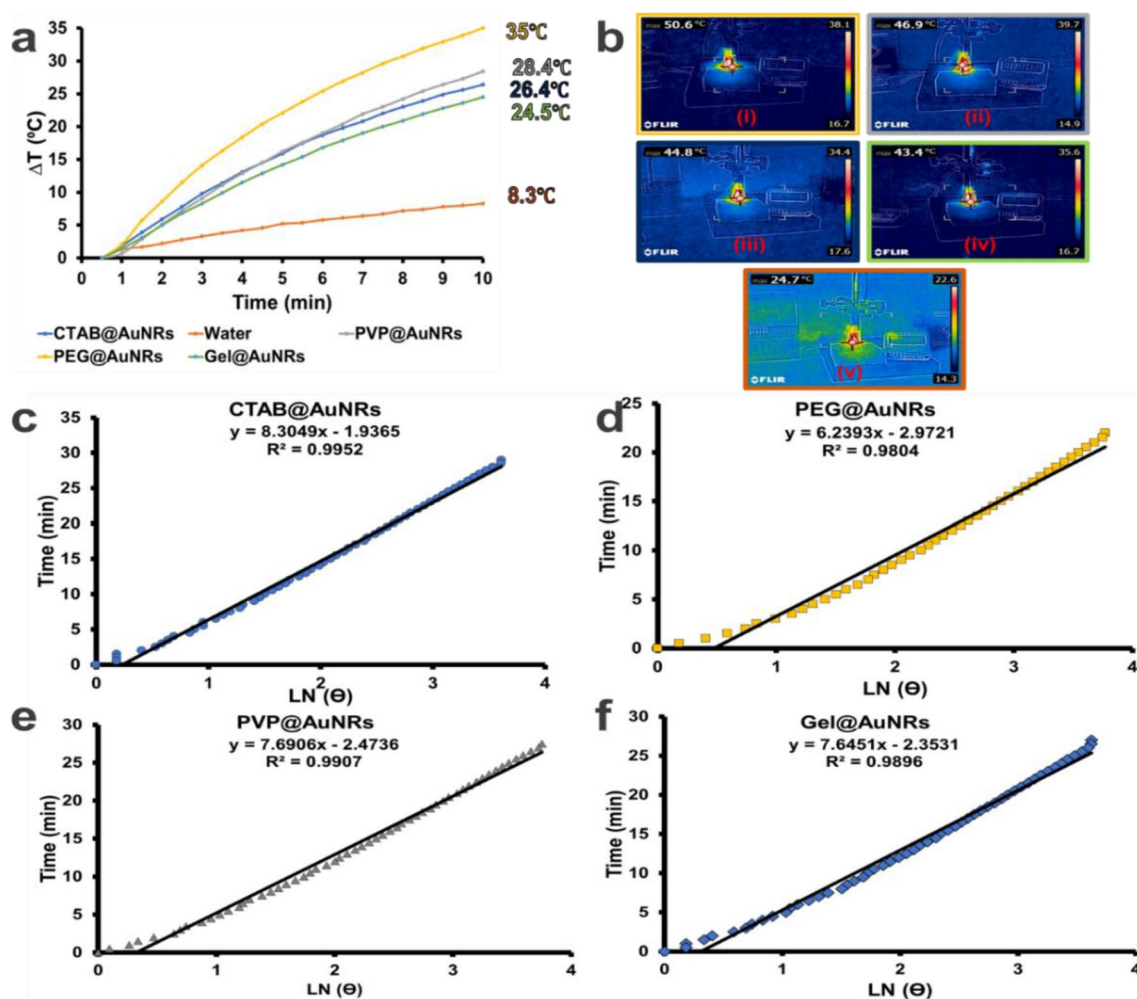
Fig. 8 a Temperature changes of deionised water, CTAB@AuNRs, PVP@AuNRs, PEG@AuNRs and Gel@AuNRs after irradiating with 808 nm Laser (power density = 2.98 W/cm^2) overtime for 10 min. **b** Thermal images of (i) PEG@AuNRs, (ii) PVP@AuNRs, (iii) CTAB@AuNRs, (iv) Gel@AuNRs and (v) deionised water after irradiating with 808 nm Laser (power = 1.5 W) for 10 min. Linear plot of the natural logarithm of temperature change versus time for **c** CTAB@AuNRs, **d** PVP@AuNRs, **e** PEG@AuNRs and **f** Gel@AuNRs

respectively. The PVP@AuNRs did not show any significant change. The Gel@AuNRs hydrodynamic size showed the presence of aggregation compared to other stabilisers. The mediun stability study showed that PEG@AuNRs was the most stable in RPMI and PBS because it does not easily bind with proteins and other ions compared to PVP@AuNRs and Gel@AuNRs with high electronegative functional groups. PVP@AuNRs was more thermally stable than the other stabilisers, because PVP has a higher decomposition temperature; hence it protected the AuNRs from deformation. On the other hand, Gel@AuNRs was the least because of the gelatin's lower dissociation temperature. The heat-generating capacity of the as-synthesised nanomaterial showed that coating materials did not affect the AuNRs' ability to produce heat. However, PEG@AuNRs had the ability to improve the heat-generating capacity and photothermal conversion efficiency compared to the other stabilisers. This study demonstrated that the coating of AuNRs with PVP, PEG, or gelatin differed. Based on the data, PVP and PEG are the best choices for coating applications in photothermal treatment. Furthermore, we recommend that polymers with fewer functional groups are chosen when coating nanoparticles to avoid protein and ion binding for biological applications. In addition, other thiolated polymers may be investigated to determine if the output will be similar to the PEG@AuNRs.

Declarations

Conflict of interest The authors declare no conflict of interest.

Data Availability The data that support the finding of this study are available from the corresponding author upon reasonable request.

References

1. X. Shi, H.L. Perry, J.D. Wilton-Ely, Strategies for the functionalisation of gold nanorods to reduce toxicity and aid clinical translation. Nanotheranostics **5**, 155 (2021). https://doi.org/10.7150/ntno.56432

2. L. Meng, J. Zhang, H. Li, W. Zhao, T. Zhao, Preparation and progress in application of gold nanorods. J. Nanomater. **2019**, 4925702 (2019). https://doi.org/10.1155/2019/4925702

3. L.C. Kennedy, L.R. Bickford, N.A. Lewinski et al., A new era for cancer treatment: gold-nanoparticle-mediated thermal therapies. Small **7**, 169 (2011)

4. W. Tong, M.J. Walsh, P. Mulvaney, J. Etheridge, A.M. Funston, Control of symmetry breaking size and aspect ratio in gold nanorods: underlying role of silver nitrate. J. Phys. Chem. C **121**, 3549 (2017)

5. H.-H. Chang, C.J. Murphy, Mini gold nanorods with tunable plasmonic peaks beyond 1000 nm. Chem. Mater. **30**, 1427 (2018)

6. N. Hlapisi, T.E. Motaung, L.Z. Linganiso, O.S. Oluwafemi, S.P. Songca, Encapsulation of gold nanorods with porphyrins for the potential treatment of cancer and bacterial diseases: a critical review. Bioinorg. Chem. Appl. **2019**, 7147128 (2019)

7. Y. Li, Z. Li, W. Ye et al., Gold nanorods and graphene oxide enhanced BSA-AgInS2 quantum dot-based photoelectrochemical sensors for detection of dopamine. Electrochim. Acta **295**, 1006 (2019)

8. J. Choi, S.Y. Kim, Photothermally enhanced photodynamic therapy based on glutathione-responsive pheophorbide a-conjugated gold nanorod formulations for cancer theranostic applications. J. Ind. Eng. Chem. **85**, 66 (2020). https://doi.org/10.1016/j.jiec.2020.01.018

9. K.I. Requejo, A. Liopo, E.R. Zubarev, Gold nanorods synthesis with small thiolated molecules. Langmuir **36**, 3758–3769 (2020)

10. Q. Zong, N. Dong, X. Yang, G. Ling, P. Zhang, Development of gold nanorods for cancer treatment. J. Inorg. Biochem. **220**, 111458 (2021). https://doi.org/10.1016/j.jinorgbio.2021.111458

11. T.C. Lebepe, S. Parani, O.S. Oluwafemi, Graphene oxide-coated gold nanorods: synthesis and applications. Nanomaterials **10**, 2149 (2020). https://doi.org/10.3390/nano10112149

12. T.C. Lebepe, O.S. Oluwafemi, Thermal and medium stability study of polyvidone-modified graphene oxide-coated gold nanorods with high photothermal efficiency. Nanomaterials **12**, 3382 (2022)

13. A.P. Leonov, J. Zheng, J.D. Clogston, S.T. Stern, A.K. Patri, A. Wei, Detoxification of gold nanorods by treatment with polystyrenesulfonate. ACS Nano **2**, 2481 (2008). https://doi.org/10.1021/nn800466c

14. I.P. Lau, H. Chen, J. Wang et al., In vitro effect of CTAB-and PEG-coated gold nanorods on the induction of eryptosis/erythroptosis in human erythrocytes. Nanotoxicology **6**, 847 (2012). https://doi.org/10.3109/17435390.2011.625132

15. A.O. Oladipo, T.C. Lebepe, V. Ncapayi et al., The therapeutic effect of second near-infrared absorbing gold nanorods on metastatic lymph nodes via lymphatic delivery system. Pharmaceutics **13**, 1359 (2021). https://doi.org/10.3390/pharmaceutics13091359

16. R. Terracciano, A. Zhang, M.L. Simeral, D. Demarchi, J.H. Hafner, C.S. Filgueira, Improvements in gold nanorod biocompatibility with sodium dodecyl sulfate stabilization. J. Nanotheranostics **2**, 157 (2021)

17. N.N. Mahmoud, H. Aqabani, S. Hikmat, R. Abu-Dahab, Colloidal stability and cytotoxicity of polydopamine-conjugated gold nanorods against prostate cancer cell lines. Molecules **26**, 1299 (2021)

18. E. Nandanan, N.R. Jana, J.Y. Ying, Functionalization of gold nanospheres and nanorods by chitosan oligosaccharide derivatives. Adv. Mater. **20**, 2068 (2008). https://doi.org/10.1002/adma.200702193

19. C. Borri, S. Centi, F. Ratto, R. Pini, Polylysine as a functional biopolymer to couple gold nanorods to tumor-tropic cells. J. Nanobiotechnol. **16**, 50 (2018). https://doi.org/10.1186/s12951-018-0377-7

20. A. Oladipo, T.C. Lebepe, S. Parani et al., Synthesis of NIR-II absorbing gelatin stabilized gold nanorods and its photothermal therapy application against fibroblast histiocytoma cells. Pharmaceuticals **14**, 1137 (2021)

21. C. Grabinski, N. Schaeublin, A. Wijaya et al., Effect of gold nanorod surface chemistry on cellular response. ACS Nano **5**, 2870 (2011). https://doi.org/10.1021/nn103476x

22. B. Zhu, J. Shi, C. Liu, J. Li, S. Cao, In-situ self-assembly of sandwich-like Ti3C2 MXene/gold nanorods nanosheets for synergistically enhanced near-infrared responsive drug delivery. Ceram. Int. **47**, 24252 (2021). https://doi.org/10.1016/j.ceramint.2021.05.136

23. J.C.Y. Kah, J. Chen, A. Zubieta, K. Hamad-Schifferli, Exploiting the protein corona around gold nanorods for loading and triggered release. ACS Nano **6**, 6730 (2012). https://doi.org/10.1021/nn301389c

24. M. Tebbe, C. Kuttner, M. Männel, A. Fery, M. Chanana, Colloidally stable and surfactant-free protein-coated gold nanorods in biological media. ACS Appl. Mater. Interfaces **7**, 5984 (2015). https://doi.org/10.1021/acsami.5b00335

25. A. Jakhmola, R. Vecchione, V. Onesto et al., A theoretical and experimental study on L-tyrosine and citrate mediated sustainable production of near infrared absorbing twisted gold nanorods. Mater. Sci. Eng. C **118**, 111515 (2021)

26. M.S. Khan, S. Pandey, M.L. Bhaisare, G. Gedda, A. Talib, H.-F. Wu, Graphene oxide@gold nanorods for chemo-photothermal treatment and controlled release of doxorubicin in mice Tumor. Colloids Surf. B Biointerfaces **160**, 543 (2017). https://doi.org/10.1016/j.colsurfb.2017.09.001

27. T.C. Lebepe, S. Parani, V. Ncapayi et al., Graphene oxide-gold nanorods nanocomposite-porphyrin conjugate as promising tool for cancer phototherapy performance. Pharmaceuticals **14**, 1295 (2021)

28. B. Sun, J. Wu, S. Cui et al., In situ synthesis of graphene oxide/gold nanorods theranostic hybrids for efficient tumor computed tomography imaging and photothermal therapy. Nano Res. **10**, 37 (2017). https://doi.org/10.1007/s12274-016-1264-x

29. M.S. Khan, S. Pandey, M.L. Bhaisare, G. Gedda, A. Talib, H.-F. Wu, Graphene oxide@ gold nanorods for chemo-photothermal treatment and controlled release of doxorubicin in mice Tumor. Colloids Surf. B **160**, 543 (2017)

30. S. Kumar, A. Mongia, S. Gulati, P. Singh, A. Diwan, S. Shukla, Emerging theranostic gold nanostructures to combat cancer: Novel probes for combinatorial immunotherapy and photothermal therapy. Cancer Treat. Res. Commun. **25**, 100258 (2020)

31. Q. Wei, H. Ni, X. Jin, J. Yuan, Graphene oxide wrapped gold nanorods for enhanced photothermal stability. RSC Adv. **5**, 54971 (2015). https://doi.org/10.1039/C5RA08333H

32. U. Dembereldorj, S.Y. Choi, E.O. Ganbold et al., Gold nanorod-assembled PEGylated graphene-oxide nanocomposites for photothermal cancer therapy. Photochem. Photobiol. **90**, 659 (2014). https://doi.org/10.1111/php.12212

33. D.-K. Lim, A. Barhoumi, R.G. Wylie, G. Reznor, R.S. Langer, D.S. Kohane, Enhanced photothermal effect of plasmonic nanoparticles coated with reduced graphene oxide. Nano Lett. **13**, 4075 (2013). https://doi.org/10.1021/nl4014315

34. Z. Qi, J. Shi, B. Zhu, J. Li, S. Cao, Gold nanorods/graphene oxide nanosheets immobilized by polydopamine for efficient remotely triggered drug delivery. J. Mater. Sci. **55**, 14530 (2020). https://doi.org/10.1007/s10853-020-05050-2

35. T. Zhao, X. Shen, L. Li et al., Gold nanorods as dual photo-sensitizing and imaging agents for two-photon photodynamic therapy. Nanoscale **4**, 7712 (2012)

36. D. Maccora, V. Dini, C. Battocchio et al., Gold nanoparticles and nanorods in nuclear medicine: A mini review. Appl. Sci. **9**, 3232 (2019)

37. T. Niidome, A. Ohga, Y. Akiyama et al., Controlled release of PEG chain from gold nanorods: Targeted delivery to tumor. Biorg. Med. Chem. **18**, 4453 (2010). https://doi.org/10.1016/j.bmc.2010.04.070

38. R. Zou, Q. Zhang, Q. Zhao et al., Thermal stability of gold nanorods in an aqueous solution. Colloids Surf. Physicochem. Eng. Aspects **372**, 177 (2010). https://doi.org/10.1016/j.colsurfa.2010.10.012

39. X. Li, J. Zhou, X. Dong, W.-Y. Cheng, H. Duan, P.C.K. Cheung, In vitro and in vivo photothermal cancer therapeutic effects of gold nanorods modified with mushroom β-glucan. J. Agric. Food Chem. **66**, 4091 (2018). https://doi.org/10.1021/acs.jafc.8b00292

40. H. Liu, N. Pierre-Pierre, Q. Huo, Dynamic light scattering for gold nanorod size characterization and study of nanorod–protein interactions. Gold Bull. **45**, 187 (2012). https://doi.org/10.1007/s13404-012-0067-4

41. H. Chen, X. Kou, Z. Yang, W. Ni, J. Wang, Shape-and size-dependent refractive index sensitivity of gold nanoparticles. Langmuir **24**, 5233 (2008)

42. H.J. Kim, J.M. Lee, J.H. Choi, D.H. Kim, G.S. Han, H.S. Jung, Synthesis and adsorption properties of gelatin-conjugated hematite (α-Fe_2O_3) nanoparticles for lead removal from wastewater. J. Hazard. Mater. **416**, 125696 (2021). https://doi.org/10.1016/j.jhazmat.2021.125696

43. V. Canpean, A. Gabudean, S. Astilean, Enhanced thermal stability of gelatin coated gold nanorods in water solution. Colloids Surf. Physicochem. Eng. Aspects **433**, 9 (2013). https://doi.org/10.1016/j.colsurfa.2013.03.072

44. X. Zhu, W. Feng, J. Chang et al., Temperature-feedback upconversion nanocomposite for accurate photothermal therapy at facile temperature. Nat. Commun. **7**, 10437 (2016). https://doi.org/10.1038/ncomms10437

45. W. Albrecht, A. van de Glind, H. Yoshida et al., Impact of the electron beam on the thermal stability of gold nanorods studied by environmental transmission electron microscopy. Ultramicroscopy **193**, 97 (2018). https://doi.org/10.1016/j.ultramic.2018.05.006

46. Y. Du, P. Yang, Z. Mou, N. Hua, L. Jiang, Thermal decomposition behaviors of PVP coated on platinum nanoparticles. J. Appl. Polym. Sci. **99**, 23 (2006)

47. M. Wesołowska-Trojanowska, M. Tomczyńska-Mleko, K. Terpiłowski et al., Co-gelation of gluten and gelatin as a novel functional material formation method. J. Food Sci. Technol. **57**, 163 (2020). https://doi.org/10.1007/s13197-019-04042-8

48. A.A. Minea, State of the art in PEG-based heat transfer fluids and their suspensions with nanoparticles. Nanomaterials **11**, 86 (2021)

49. E. Leonidas, S. Ayvar-Soberanis, H. Laalej, S. Fitzpatrick, J.R. Willmott, A comparative review of thermocouple and infrared radiation temperature measurement methods during the machining of metals. Sensors **22**, 4693 (2022)